Journal of Power Sources 196 (2011) 7395–7403

Contents lists available at ScienceDirect

Journal of Power Sources

journal homepage: www.elsevier.com/locate/jpowsour

Phase stability and electrical conductivity of Ca-doped $LaNb_{1-x}Ta_xO_{4-\delta}$ high temperature proton conductors

Zhonghe Bi[a], Craig A. Bridges[a], Jung-Hyun Kim[b], Ashfia Huq[b], M. Parans Paranthaman[a,*]

[a] Chemical Sciences Division, Oak Ridge National Laboratory, Oak Ridge, TN 37831, United States
[b] Neutron Scattering Science Division, Oak Ridge National Laboratory, Oak Ridge, TN 37831, United States

ARTICLE INFO

Article history:
Received 1 March 2011
Received in revised form 1 April 2011
Accepted 4 April 2011
Available online 8 April 2011

Keywords:
SOFCs
High temperature proton conductor
Rare-earth ortho-niobates
Phase transition
AC conductivity

ABSTRACT

The electrical conductivity, crystal structure and phase stability of $La_{0.99}Ca_{0.01}Nb_{1-x}Ta_xO_{4-\delta}$ ($x = 0, 0.1, 0.2, 0.3, 0.4$ and 0.5, $\delta = 0.005$), a potential candidate for proton conductor for solid oxide fuel cells (SOFCs), have been investigated using AC impedance technique and in situ X-ray powder diffraction. Partially substituting Nb with Ta elevates the phase transition temperature (from a monoclinic to a tetragonal structure) from ~520 °C for $x = 0$ to above 800 °C for $x = 0.4$. AC conductivity of the $La_{0.99}Ca_{0.01}Nb_{1-x}Ta_xO_{4-\delta}$ both in dry and wet air decreased slightly with increasing Ta content above 750 °C, while below 500 °C, it decreased by nearly one order of magnitude for $x = 0.4$. It was also determined that the activation energy for the total conductivity increases with increasing Ta content from 0.50 eV ($x = 0$) to 0.58 eV ($x = 0.3$) for the tetragonal phase, while it decreases with increasing Ta content from 1.18 eV ($x = 0$) to 1.08 eV ($x = 0.4$) for the monoclinic phase. By removing the detrimental structural phase transition from the intermediate-temperature range, consequently avoiding the severe thermal expansion problem up to 800 °C, partial substitution of Nb with Ta brings this class of material closer to its application in electrode-supported thin-film intermediate-temperature SOFCs.

Published by Elsevier B.V.

1. Introduction

High-temperature proton conducting ceramics have numerous industrial applications such as solid oxide fuel cells, gas separation membranes, gas sensors and hydrogenation/dehydrogenation of hydrocarbons [1–3]. Perovskites containing Ba and Sr such as $Ba/SrCeO_3$ exhibit state-of-the-art proton conductivity of about $0.01\ S\,cm^{-1}$, however, the relatively poor chemical and mechanical stabilities in CO_2 and H_2O containing atmospheres limits their applications in the commercial market [4,5]. Recently, a new family of materials namely the Ca-doped rare-earth ortho-niobates and ortho-tantalates was reported by Haugsrud and Norby, with maximum proton conductivity close to $10^{-3}\ S\,cm^{-1}$ for 1% Ca-doped $LaNbO_{4-\delta}$. This represents the highest level of proton conductivity in an oxide without Ba or Sr as the main components; in addition, these materials are expected to show much better chemical stability in CO_2 containing atmospheres [6–8]. The relatively low proton conductivity requires that the electrolyte thickness should be in the order of μm-scale to obtain an acceptable performance for high-temperature fuel cell application. Recently, thin-film fabrication techniques have been successfully applied for fabricating Sr or Ca-doped $LaNbO_{4-\delta}$ thin films, which have exhibited the potential for future commercial applications [9–11]. However, the reversible phase transformation in $LaNbO_{4-\delta}$ from the monoclinic fergusonite crystal structure at low temperature to a tetragonal structure at high temperature occurs at 495–525 °C, and is detrimental to high performance applications [12,13]. According to the previous study, the thermal expansion coefficient of $LaNbO_{4-\delta}$ is strongly influenced by the phase transition from low temperature monoclinic phase to high temperature tetragonal phase. Although the phase transformation in $LaNbO_{4-\delta}$ is considered to be second order in nature and the volume change is continuous, a discontinuous change in the line and volume thermal expansion coefficients (TECs) was observed, which showed a value of approximately $17.3 \pm 0.5 \times 10^{-6}\ K^{-1}$ for the monoclinic phase and $7.1 \pm 0.7 \times 10^{-6}\ K^{-1}$ for the tetragonal phase, respectively [14,15]. This huge TEC difference is expected to lead to a serious problem during thermal cycling of the electrochemical device with Ca-doped $LaNbO_{4-\delta}$ as the electrolyte.

According to earlier studies, the phase transition temperatures increase with decreasing radii of the rare-earth (RE) cations in the temperature range of 500–830 °C, which are much lower than that observed for the iso-structural $RETaO_4$ (1300–1450 °C) [12]. Therefore, partial or full substitution of Nb with Ta offers a path to change the phase transition temperature, in order to increase the temperature range at which these materials will prove to exhibit a stable

* Corresponding author. Tel.: +1 865 574 5045; fax: +1 865 574 4961.
E-mail address: paranthamanm@ornl.gov (M.P. Paranthaman).

0378-7753/$ – see front matter. Published by Elsevier B.V.
doi:10.1016/j.jpowsour.2011.04.006

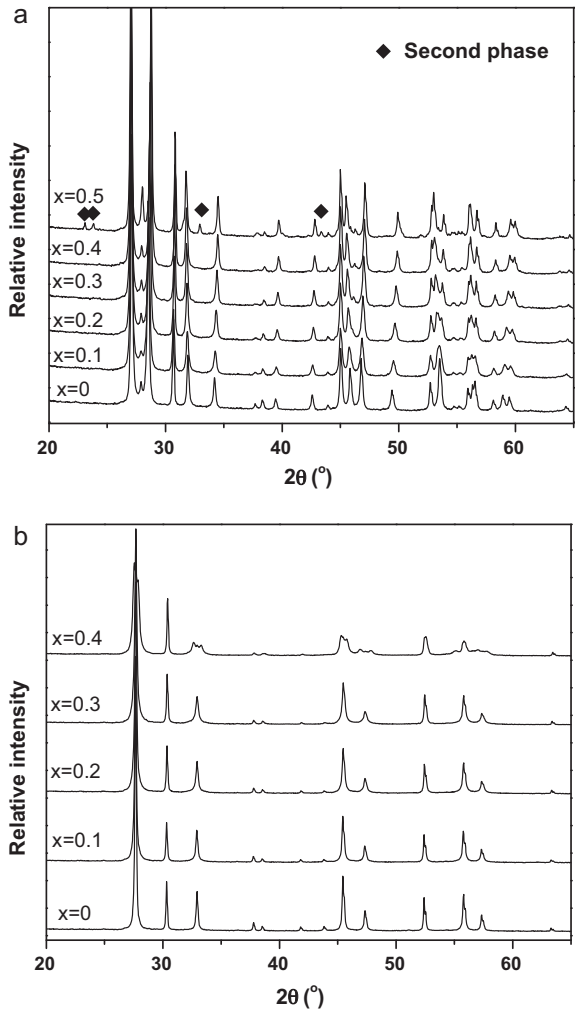

Fig. 1. XRD patterns of $La_{0.99}Ca_{0.01}Nb_{1-x}Ta_xO_{4-\delta}$ phases obtained (a) at room temperature (♦ indicating the second phase) and (b) at 800 °C, respectively.

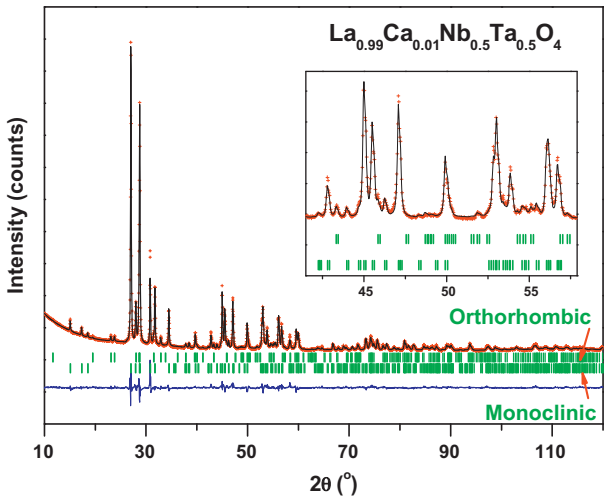

Fig. 2. Rietveld refinement results obtained from the X-ray powder diffraction data for $La_{0.99}Ca_{0.01}Nb_{0.5}Ta_{0.5}O_{4-\delta}$ at room temperature.

crystal structure [12]. Unfortunately, the electrical conductivity of 1 mol% Ca-doped $RETaO_{4-\delta}$ (RE = La, Nd, Gd, and Er) only exhibited a maximum proton conductivity of $\sim 3 \times 10^{-4}$ S cm^{-1} for $LaTaO_4$ at 1000 °C, which is about one tenth of the 1 mol% Ca-doped $LaNbO_{4-\delta}$ at 800 °C [16]. Hence, it is interesting to investigate the influence of partially substituting Nb with Ta on the structural and electrical properties of 1 mol% Ca-doped $LaNbO_{4-\delta}$, as the ability to raise the phase transition temperature may outweigh a slight loss in conductivity at low doping levels. In this paper, we have undertaken a systematic study of this family of materials of Ca-doped $LaNb_{1-x}Ta_xO_{4-\delta}$ (x = 0–0.5 in steps of 0.1). We have used in situ high-temperature X-ray diffraction to study its crystal structure and structural phase transition; and AC impedance techniques to characterize its electrochemical properties in order to evaluate its suitability as an electrolyte material for high-temperature electrochemical device applications.

2. Experimental

All powders of $La_{0.99}Ca_{0.01}Nb_{1-x}Ta_xO_{4-\delta}$ (x = 0, 0.1, 0.2, 0.3, 0.4 and 0.5) were synthesized by a conventional solid-state reaction method. Stoichiometric amounts of dried La_2O_3 (Alfa Aesar, 99.99%), Nb_2O_5 (Alfa Aesar, 99.99%), Ta_2O_5 (Alfa Aesar, 99.85%) and $CaCO_3$ (Alfa Aesar, 99.9%) were mixed thoroughly in an Al_2O_3 mortar, then pelletized and fired at 1150 °C for 10 h, followed by grinding using mortar and pestle, then fired at 1250 °C for 10 h, with a second regrinding and pelletizing and finally firing at 1500–1550 °C for 10 h. Phase purity and stability were characterized using a Philips X'pert Pro powder X-ray diffractometer equipped with an X'Celerator detector, using Cu-Kα radiation (λ = 1.5418 Å). All diffraction data analyses were performed using the program package GSAS [17,18].

Dense pellets were obtained with relative density higher than 93% after sintering at 1500–1550 °C for 10 h. The as-sintered pellets were ground and polished to a thickness of 850 μm using a SiC paper for AC conductivity measurements. Two symmetrical porous Pt electrodes of diameter 7.0 mm were applied directly to both sides of the pellets by painting with two layers of Pt paint (Heans 901) on each side, then dried and fired at 900 °C for 0.5 h in air. Pt mesh with Pt wire was placed on the electrode surface to complete the electrical connections. The assembled cell was placed in a quartz reactor which was supported in a tubular furnace. The air gas was either passed through the silica–gel dryer directly (designated as "dry") or humidified to ~2.7 mol% water content by passing through a water bubbler kept at room temperature. Flow rates were 50 ml min^{-1} for both dry and humidified air. A standard experimental procedure was followed in which the cell was heated up to 850 °C and held at this temperature for 15 h in dry air. Impedance spectra were recorded at temperature intervals down to 400 °C in dry air. At each temperature point, impedance spectra were recorded at 1 h intervals until concurrent results were obtained. Then dry air was switched to humidified air and the cell was heated to 850 °C again and held for another 15 h to hydrate the samples. The AC impedance measurements were repeated with the same intervals and procedures in wet air. All heating and cooling rates were 5 °C min^{-1}. It is noted that the concurrent impedance result (difference was less than 0.5%) was obtained in several hours after hydrated at 850 °C, since the hydration of oxygen vacancies is relatively slow below 800 °C, requiring about one week to obtain equilibrium during hydration at 760 °C [19]. Impedance spectra were recorded in the frequency range 10^6–0.01 Hz with signal amplitude of 100 mV using VersaSTAT 4 (Princeton Applied Research) with an internal frequency response analyzer. ZSimpWin software was used to fit the acquired impedance data to equivalent circuits. Depending on the complex impedance plane plot shape, different equivalent circuits were used consisting of sub-circuits of resistors (R_i) and constant phase elements (Q_i) in parallel, denoted as (R_iQ_i). Above 600 °C, the (R_1Q_1)(R_3Q_3) equivalent circuit was used since only one low frequency depressed arc was observed. For the temperatures

in the range of 550–400 °C, the $(R_1Q_1)(R_2Q_2)(R_3Q_3)$ equivalent circuit was used due to an intermediate-frequency arc emerged in the impedance spectrum clearly.

3. Results and discussion

Fig. 1a and b shows X-ray diffraction (XRD) patterns for the $La_{0.99}Ca_{0.01}Nb_{1-x}Ta_xO_{4-\delta}$ (x = 0, 0.1, 0.2, 0.3, 0.4, 0.5) powders at room temperature and 800 °C, respectively. Note that the oxygen defect concentration (δ) resulting from calcium doping is expected to remain constant over all samples, at a level of 0.005 mol formula^{-1} unit. From the patterns obtained at room temperature shown in Fig. 1a, single monoclinic-phase powders were obtained for x = 0–0.4, however, for the composition x = 0.5 a second phase from orthorhombic $LaTaO_4$was observed. The results were in good agreement with previous reports, which showed that it is not possible to obtain phase-pure powders in the system $LaNb_{1-x}Ta_xO_4$ without Ca-doping for x = 0.6 even after numerous cycles of sintering at high temperature with intermediate grindings [15]. Also, qualitative analysis revealed that the solid solubility limits exist somewhere between $LaNb_{0.6}Ta_{0.4}O_4$ and $LaNb_{0.5}Ta_{0.5}O_4$ in the Nb-rich $LaNb_{1-x}Ta_xO_4$ system [20]. At 800 °C, the low-temperature monoclinic phase changed to the high-temperature tetragonal phase completely for the compositions where $x \leq 0.3$, as shown in Fig. 1b. However, for the x = 0.4 sample, the XRD pattern had to be analyzed by considering a two phase system composed of monoclinic and tetragonal phases at 800 °C. The mixture of phases is due to the fact that the phase transition temperature is elevated to near 800 °C from tantalum substitution, and the likelihood that there is a slight temperature gradient across the sample at this temperature. Investigation to higher temperature reveals a single phase, indicating that the mixture of phases at 800 °C is not due to compositional inhomogeneity. All the X-ray diffraction data at room temperature for the compositions $x \leq 0.4$ were fitted to a monoclinic fergusonite structure (Space Group I 1 1 2/b), and at 800 °C for $x \leq 0.3$ to a tetragonal structure (Space Group I 41/a). The room temperature X-ray diffraction data for the $La_{0.99}Ca_{0.01}Nb_{0.5}Ta_{0.5}O_{4-\delta}$ sample were fitted to a monoclinic fergusonite structure (I2/b) and an orthorhombic structure ($A2_1am$). Fig. 2 shows an excellent agreement between data and model based on a two phase Rietveld refinement. The relative proportion of the two phases is around 85% (weight fraction) for monoclinic phase and 15% for orthorhombic phase. The unit cell parameters for monoclinic $La_{0.99}Ca_{0.01}Nb_{1-x}Ta_xO_{4-\delta}$ at room temperature were obtained from refinement and shown in Table 1. The unit cell parameters of $La_{0.99}Ca_{0.01}NbO_{4-\delta}$ are slightly smaller than those previously reported by Jian et al., following the expected trend for 1% doping with the smaller Ca^{2+} cation in the present experiment [15,21,22]. All unit cell parameters of the $La_{0.99}Ca_{0.01}Nb_{1-x}Ta_xO_{4-\delta}$ are plotted as a function of Ta content in Fig. 3, with the exception of the sample $La_{0.99}Ca_{0.01}Nb_{0.6}Ta_{0.4}O_{4-\delta}$ at 800 °C; the quality of the refinement in this case was not good as the data were collected during the phase transition. It can be seen that parameters b, c and angle γ decrease with substitution of Nb for Ta, while parameter a increases accordingly. The cell volumes of $La_{0.99}Ca_{0.01}Nb_{1-x}Ta_xO_{4-\delta}$ also decrease from 331.685 Å^3 for x = 0 to 330.258 Å^3 for x = 0.5. While the ionic sizes of Nb^{5+} and Ta^{5+} are expected to be essentially identical (tabulated ionic radii are both 0.64 Å) [23], the change in volume may indicate that the size of the Ta^{5+} is actually slightly smaller in this family of materials.

The high temperature structural phase transition was investigated in more detail for the sample $La_{0.99}Ca_{0.01}Nb_{0.8}Ta_{0.2}O_{4-\delta}$ using XRD, the data were recorded from room temperature to 800 °C for a 2θ range of 10–120°. The variations in lattice parameter with increasing temperature are shown in Fig. 4. The lattice

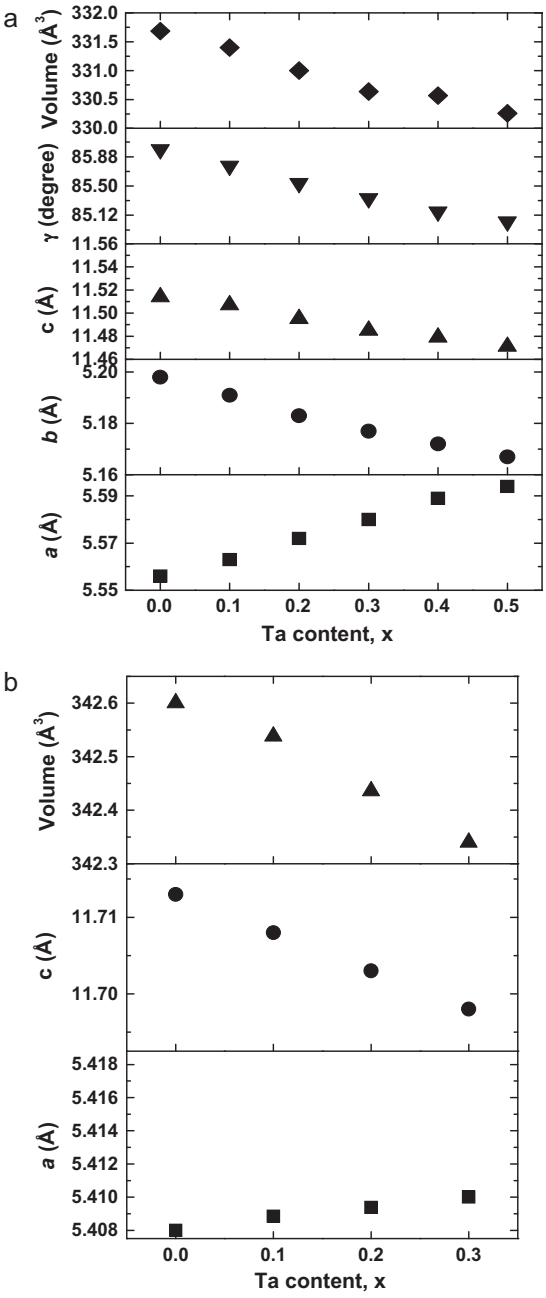

Fig. 3. Cell parameters calculated for the monoclinic phase (a) and tetragonal phase (b) as a function of Ta content in $La_{0.99}Ca_{0.01}Nb_{1-x}Ta_xO_{4-\delta}$.

parameter a decreases with increasing temperature, while the lattice parameter b increases (Fig. 4a); as a result the a and b axes are seen to converge at the phase transition temperature (near 675 °C). Similarly, the monoclinic angle γ asymptotically increases with temperature and approaches 90° nearing the phase transition temperature (Fig. 4b). An estimate of the phase transition temperature from Landau theory, given that the phase transition is second order, by plotting the square of the monoclinic strain $(ab\cos\gamma)^2$ versus temperature (Fig. 4c) [24]. The data near to the phase transition follow a linear trend with temperature, allowing an estimate of 679(13) °C for the transition temperature from a least squares fit. From Fig. 4d, the cell volume increases continuously but a different slope is observed in monoclinic and tetragonal phases. This indicates the thermal expansion coefficient (TEC) is much different below and above phase transition temperatures.

Table 1
Cell parameters for monoclinic phase at room temperature, phase transition temperatures (T_{trs}) and activation energies (E_a) for $La_{0.99}Ca_{0.01}Nb_{1-x}Ta_xO_{4-\delta}$.

	a (Å)	b (Å)	c (Å)	γ (°)	T_{trs} (°C) fitted from Arrhenius plots	E_a (eV) for monoclinic	E_a (eV) for tetragonal
$x=0$	5.555(2)	5.1982(1)	11.5139(3)	85.97(2)	524 ± 10	1.180	0.502
$x=0.1$	5.563(3)	5.191(3)	11.506(7)	85.76(3)	594 ± 10	1.171	0.520
$x=0.2$	5.572(2)	5.183(2)	11.495(5)	85.54(2)	672 ± 10	1.130	0.525
$x=0.3$	5.580(2)	5.176(2)	11.485(5)	85.34(2)	760 ± 10	1.100	0.585
$x=0.4$	5.588(2)	5.172(2)	11.479(5)	85.16(2)	>800	1.080	–
$x=0.5$	5.594(1)	5.167(1)	11.471(3)	85.04(2)	–	–	–

The calculated average linear TECs for monoclinic and tetragonal phases are $17.5 \pm 0.2 \times 10^{-6}\,°C^{-1}$ and $9.5 \pm 0.1 \times 10^{-6}\,°C^{-1}$, respectively. These results are consistent with the previous reports [15]. It should be noted that the data were fitted as a two phase refinement above 600 °C, including a component of the tetragonal structure. The refined fraction of tetragonal phase varied from ~10 wt% at 600 °C to ~30 wt% at 675 °C, near to the transition. As the transition temperature is approached a prominent peak anisotropy developed, which is readily observed by comparing the relatively sharp (0 0 4) reflection (2θ, ~30.7°) and the broader (2 0 0)/(0 2 0) reflections (2θ, ~33.2°); the anisotropy indicates a greater spread in lattice parameters in the *ab* plane than along the *c* axis as the monoclinic angle approaches 90° at the transition. Though large anisotropic broadening persists above the transition there is no visible evidence in the data above 700 °C for a second phase, such that the anisotropic broadening may be related to significant residual strain in the *ab* plane above the transition. The appearance of a mixed phase region may relate partly to a temperature gradient across the sample, and also to the clustering of niobium or tantalum site occupancy, which on a larger length scale may be viewed as a slight compositional inhomogeneity. Nonetheless, a clear trend in increased phase transition temperature is observed with tantalum doping, in agreement with previous reports [15]. By elevating the phase transition temperature of $La_{0.99}Ca_{0.01}NbO_{4-\delta}$ to above 800 °C so as to remove the detrimental change in thermal expansion coefficient, the partial substitution of Nb with Ta ($x = 0.4$) improves

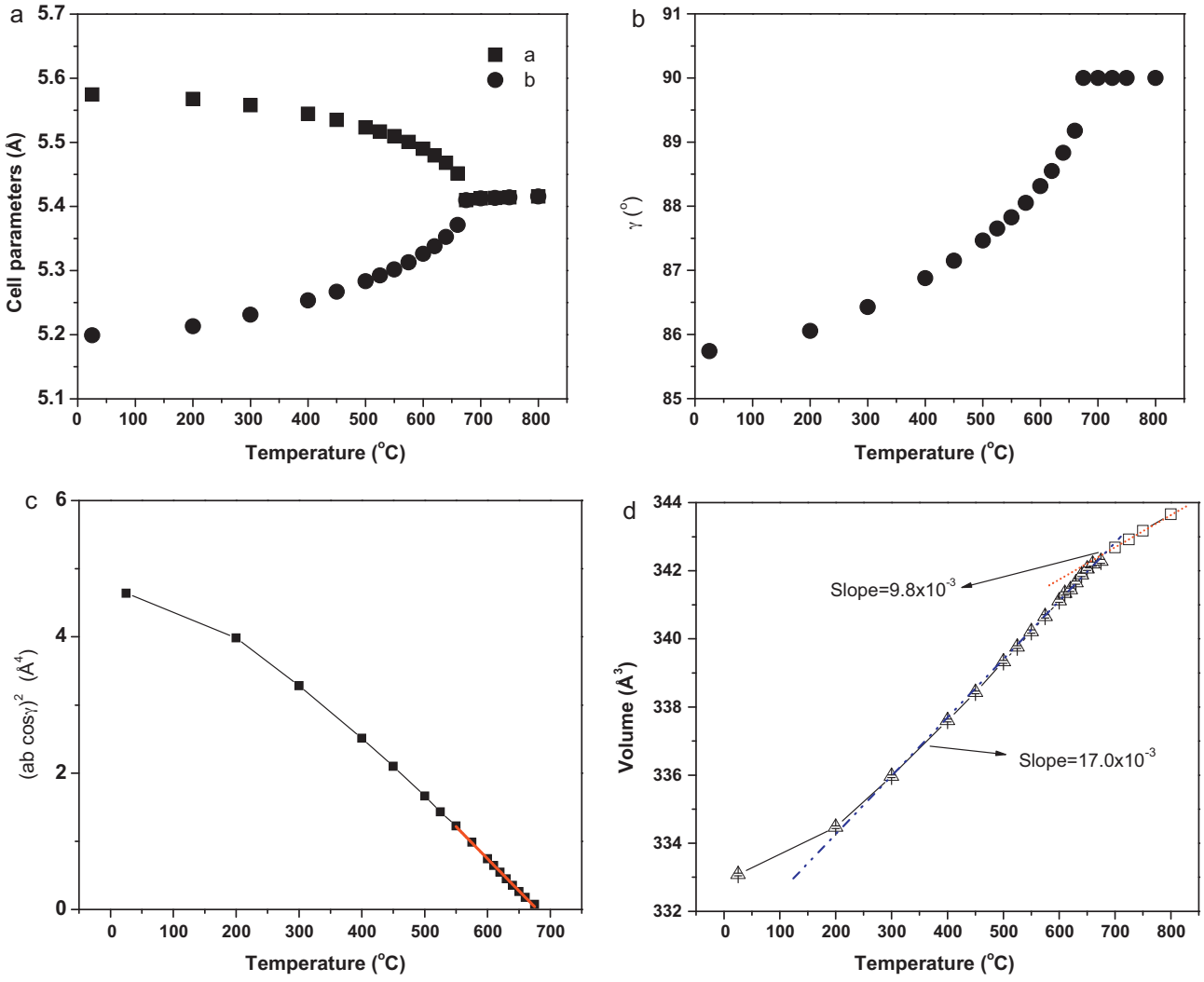

Fig. 4. Variation of (a) *a* and *b* lattice parameters, (b) γ angle, (c) the square of monoclinic strain ($ab\cos\gamma$), (d) cell volume with temperature for $La_{0.99}Ca_{0.01}Nb_{0.8}Ta_{0.2}O_{4-\delta}$ refined from in situ high-temperature X-ray diffraction data.

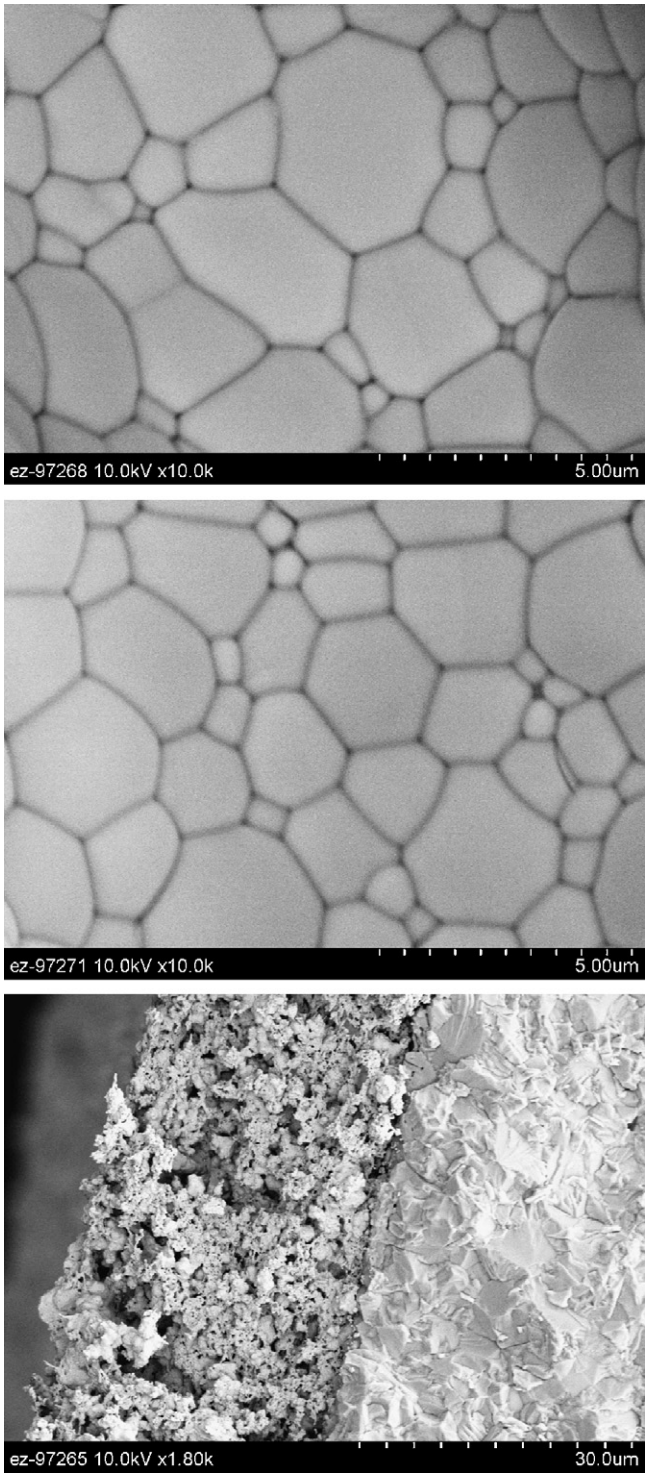

Fig. 5. SEM images for surface morphologies of (a) $La_{0.99}Ca_{0.01}Nb_{0.9}Ta_{0.1}O_{4-\delta}$ and (b) $La_{0.99}Ca_{0.01}Nb_{0.8}Ta_{0.2}O_{4-\delta}$; (c) typical cross-sectional views of the fractured $Pt/La_{0.99}Ca_{0.01}NbO_{4-\delta}/Pt$ cell after AC conductivity measurement.

the viability of these phases for application in solid oxide fuel cells operating at intermediate-temperatures.

The surface morphologies of $La_{0.99}Ca_{0.01}Nb_{0.9}Ta_{0.1}O_{4-\delta}$ and $La_{0.99}Ca_{0.01}Nb_{0.8}Ta_{0.2}O_{4-\delta}$ sintered at 1500 and 1550 °C for 10 h are selected and shown in Fig. 5a and b. A small amount of porosity along the grain boundaries was observed at the exposed surface for all of the compositions. The average grain sizes were ca. 3 μm for all the samples. A similar microstructure has also been observed

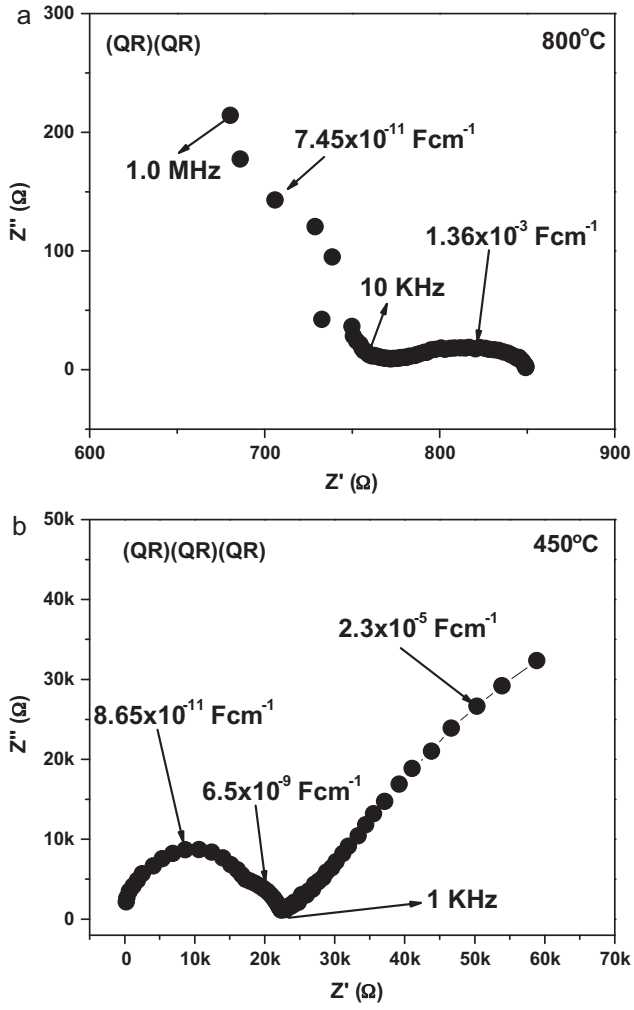

Fig. 6. AC impedance spectra for $La_{0.99}Ca_{0.01}NbO_{4-\delta}$ in wet air at (a) 800 °C and (b) 450 °C.

for Ca-, Sr- or Ba-doped $LaNbO_4$ by Mokkelbost et al. [25]. Typical cross-sectional views of the fractured $Pt/La_{0.99}Ca_{0.01}NbO_{4-\delta}/Pt$ cell near the Pt electrode side after an AC conductivity measurement is shown in Fig. 5c. The $La_{0.99}Ca_{0.01}NbO_{4-\delta}$ is quite dense with small amount of no-cross membrane pin-holes. The Pt paste layer shows a good porosity with a thickness of ~25 μm.

The impedance spectra obtained in dry and humidified air at different temperatures were modeled as an equivalent circuit, and resistance and capacitance values were extracted for the bulk, grain boundary, and overall electrodes. Above 600 °C, only one high-frequency arc and one low-frequency depressed arc were observed. Below 550 °C, however, one intermediate-frequency arc could be seen clearly. As examples, the impedance spectra obtained in humidified air at 800 and 450 °C are shown in Fig. 6a and b. Since the geometrical capacitance of the (R_1Q_1) sub-circuit (high frequency arc) was calculated to be $\sim 10^{-11}$ F cm^{-2}, R_1 has been assigned to represent the bulk resistance. For the intermediate-frequency arc (R_2Q_2) that existed below 550 °C, the capacitance value is $\sim 10^{-9}$ F cm^{-2}, which is around two orders of magnitude higher than that of bulk; therefore R_2 has been assigned to represent the grain boundary resistance. And for the low-frequency arc, the capacitance value is at the range of 10^{-3}–10^{-6} F cm^{-2}, which is from the electrode process. Similar AC impedance results about the capacitance value involving high temperature proton conductors were reported by Ahmed, Potter, and Gallini [26–28].

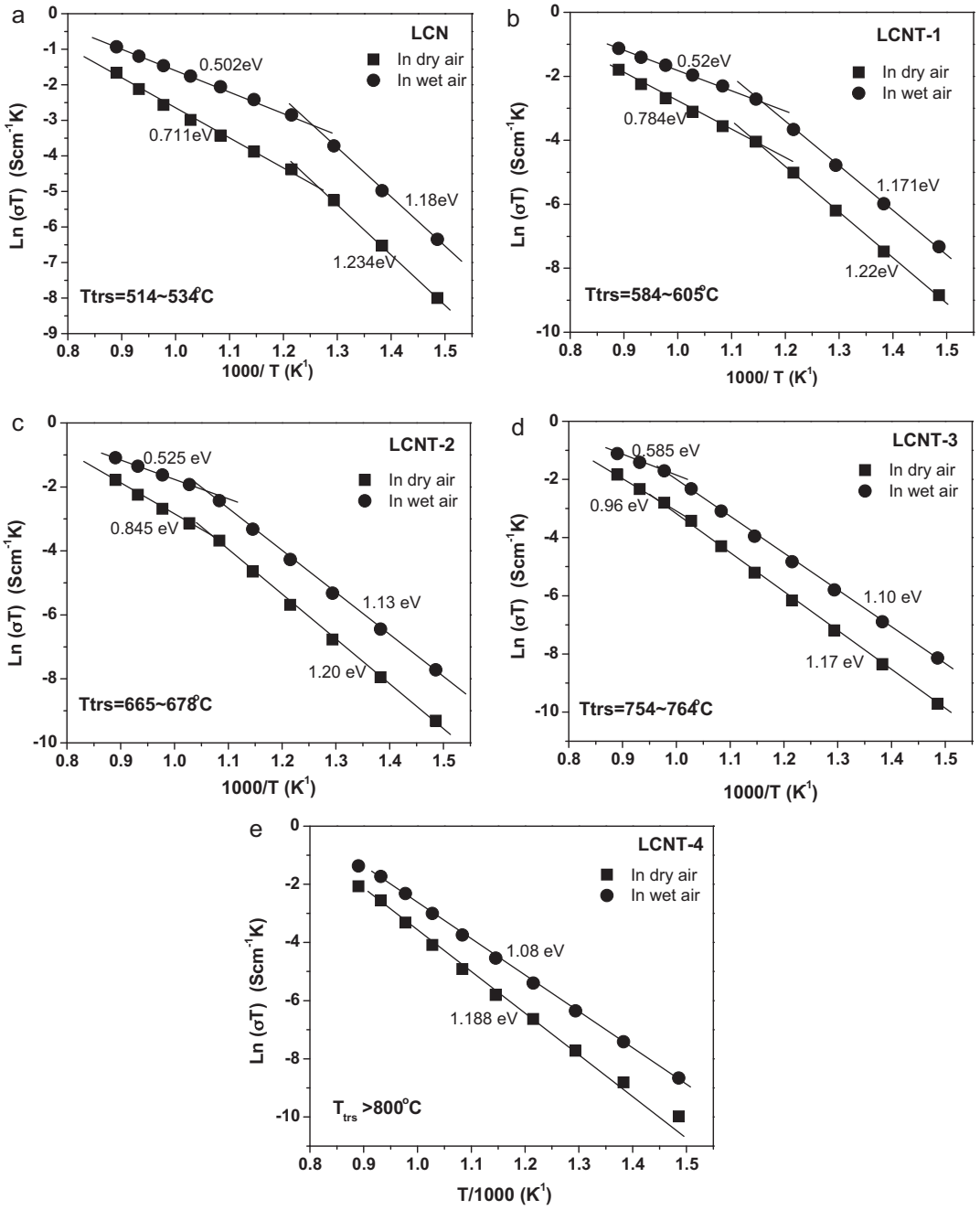

Fig. 7. Arrhenius plots for the total AC conductivity of the Pt/$La_{0.99}Ca_{0.01}Nb_{1-x}Ta_xO_{4-\delta}$/Pt cells both in dry and humidified air for (a) $x = 0$ (LCN); (b) $x = 0.1$ (LCNT-1); (c) $x = 0.2$ (LCNT-2); (d) $x = 0.3$ (LCNT-3); and (e) $x = 0.4$ (LCNT-4).

The total conductivity data from the impedance spectra of the $La_{0.99}Ca_{0.01}Nb_{1-x}Ta_xO_{4-\delta}$ ($x = 0$, 0.1, 0.2, 0.3, 0.4) samples versus inverse temperature in dry and humidified air are shown in Fig. 7. According to the previous studies, the conductivity is predominantly ionic in air below 800 °C for both Ca-doped $LaNbO_4$ and $LaTaO_4$ [7]. From Fig. 7a–e, the total AC conductivity data in wet air are much higher than that in dry air due to the fact that proton conductivity arises with incorporation of water into the samples to form hydroxide species in humidified conditions [29,30]. A break in the slope of the total conductivity around 520 °C was observed in Fig. 7a, which coincides with the monoclinic-to-tetragonal phase transition of $LaNbO_{4-\delta}$ [12,14,15]. Clearly the break point in the slopes of the total conductivity is elevated with increasing Ta content. It is elevated from around 520 °C for $x = 0$ to 775 °C for $x = 0.3$. However, for $x = 0.4$, no break was observed in the slope of the total conductivity below 800 °C, which indicates that the phase transition temperature is higher than 800 °C. All the phase transition temperatures of the $La_{0.99}Ca_{0.01}Nb_{1-x}Ta_xO_{4-\delta}$ ($x \leq 0.3$) can be obtained from the Arrhenius plots, which are in agreement with the XRD results very well, as well as for the $LaNb_{1-x}Ta_xO_{4-\delta}$ ($x = 0.2$ and 0.4) without Ca doping [15]. For comparison the phase transition temperatures (T_{trs}) of $La_{0.99}Ca_{0.01}Nb_{1-x}Ta_xO_{4-\delta}$ were summarized in Table 1. These results are promising in that electrochemical devices incorporating a thin film of $La_{0.99}Ca_{0.01}Nb_{1-x}Ta_xO_{4-\delta}$ can be operated without a huge TEC change in the intermediate operation temperature range. However, the conductivities of the series $La_{0.99}Ca_{0.01}Nb_{1-x}Ta_xO_{4-\delta}$ decreased clearly with an increase in Ta content (Fig. 7). For

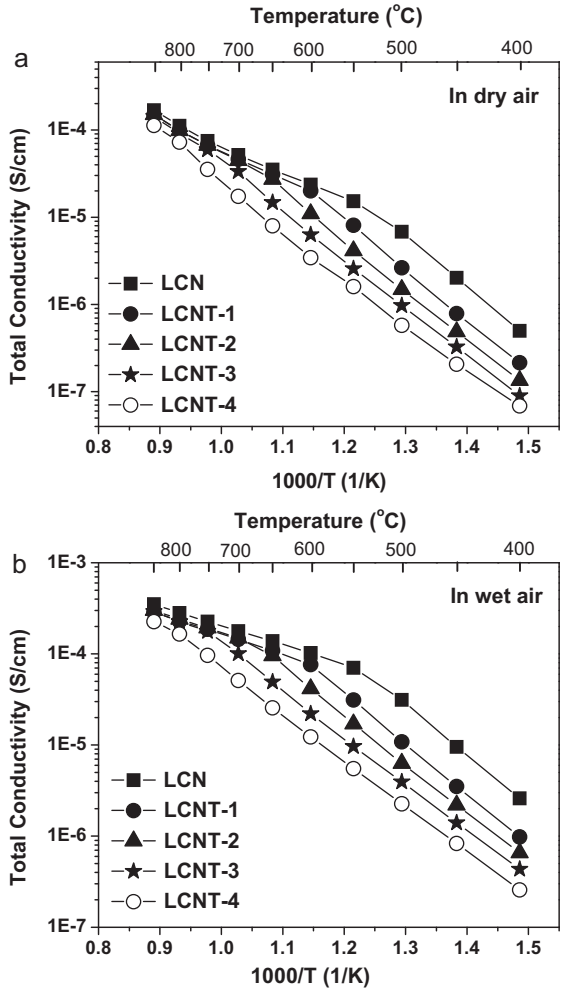

Fig. 8. Total AC conductivities of $La_{0.99}Ca_{0.01}Nb_{1-x}Ta_xO_{4-\delta}$ ($x = 0$ (LCN); $x = 0.1$ (LCNT-1); $x = 0.2$ (LCNT-2); $x = 0.3$ (LCNT-3); and $x = 0.4$ (LCNT-4)) as a function of inverse temperature in (a) dry and (b) humidified air.

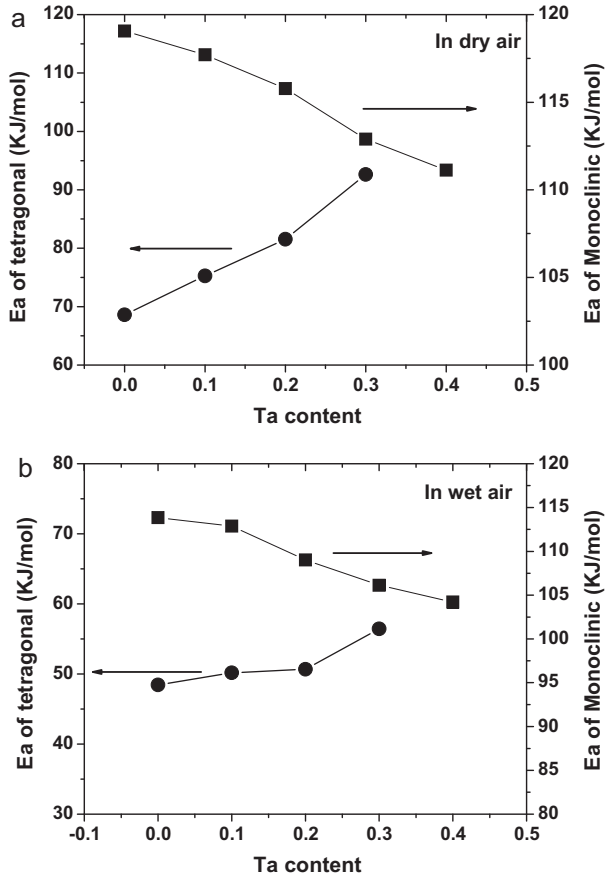

Fig. 9. Activation energies of monoclinic and tetragonal phases for $La_{0.99}Ca_{0.01}Nb_{1-x}Ta_xO_{4-\delta}$ as a function of Ta content in (a) dry and (b) humidified air.

comparison, the total conductivities versus inverse temperature in dry and humidified air are plotted in Fig. 8a and b, respectively. The phase $La_{0.99}Ca_{0.01}NbO_{4-\delta}$ exhibited a conductivity of 3.5×10^{-4} S cm^{-1} in wet air at 850 °C, while it is little lower than 1.0×10^{-3} S cm^{-1} in wet H_2 [7,8]. With the temperature decreased to 500 °C, the conductivity dropped to 1.0×10^{-4} S cm^{-1} in humidified air. For the sample $La_{0.99}Ca_{0.01}Nb_{0.6}Ta_{0.4}O_{4-\delta}$, no dramatic drop in the conductivity was observed down to 750 °C, however, below this temperature, the conductivity rapidly decreases by one order of magnitude as compared to $La_{0.99}Ca_{0.01}NbO_{4-\delta}$ both in dry and humidified air. It should be noted that while the conductivity reported in the present work was based upon measurements performed in air, the conductivity is expected to increase with increasing hydration and decreasing oxygen partial pressure [7,8]. In addition, it is clear from the temperature dependence that there is a distinct change in the activation energy for the total conductivity at the phase transition temperatures, with the exception of the sample $La_{0.99}Ca_{0.01}Nb_{0.6}Ta_{0.4}O_{4-\delta}$ which exhibits no phase transition. The activation energies (E_a) of the series $La_{0.99}Ca_{0.01}Nb_{1-x}Ta_xO_{4-\delta}$ for different crystal structures in dry and humidified air were calculated and plotted in Fig. 9 as a function of composition. It can be seen that the E_a of $La_{0.99}Ca_{0.01}Nb_{1-x}Ta_xO_{4-\delta}$ in the tetragonal phase slightly increases from 0.50 eV for $x = 0$ to 0.58 eV for $x = 0.3$ in humidified air. These results are in good agreement with values of 0.57 ± 0.05 eV reported by Haugsrud and Fjeld [7,8]. While for monoclinic phase, the E_a decreases from 1.18 eV for $x = 0$ to 1.08 eV for $x = 0.4$ in humidified air. The E_a values of the monoclinic phase are higher than the value of 0.78 eV reported by Haugsrud [7,8] and smaller than the apparent activation energy (1.24 eV) calculated by Fjeld et al. [19]. This may partly relate to the fact that the a.c. resistance (10 kHz) data obtained in the previous studies only included the bulk resistance. In the present experiment, the conductivity data were calculated including the resistance from both bulk and grain boundary contributions. Additionally, Fjeld et al. [19] have proposed that the Arrhenius approach used here is not appropriate for the monoclinic phase, and that E_a rather increases continuously with decreasing temperature in conjunction. The increase in the activation energy is related to the increase in the monoclinic distortion (i.e. lowering of symmetry) associated with the decrease in temperature. However, results here suggest that the activation energy, as derived from an Arrhenius model, decreases with increasing tantalum substitution in the monoclinic phase. It might be expected that stabilizing the monoclinic phase over a wide temperature range with higher tantalum content would lead to a higher activation energy, in analogy with the temperature dependence. In addition, the activation energy of the tetragonal phase increases with increasing tantalum substitution, despite the presence of a monoclinic lattice distortion. According to the computational results reported by Fjeld et al. [19], the rate-determining process for migration of protons in tetrahedrally coordinated $La_{0.99}Ca_{0.01}Nb_{1-x}Ta_xO_{4-\delta}$ phases is the rotation and hopping between two stable inter-tetrahedral proton sites, and is largely confined to the *ab* plane. As protons are bound to oxygen atoms the energies associated with proton transfer are affected by the distances between stable proton sites, which are

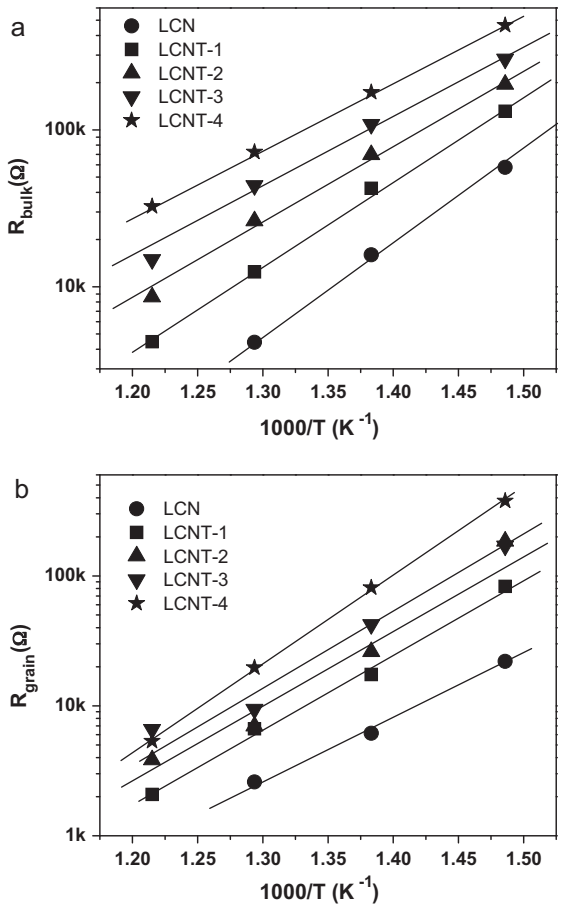

Fig. 10. Bulk (a) and grain boundary (b) resistance versus inverse temperature of the $La_{0.99}Ca_{0.01}Nb_{1-x}Ta_xO_{4-\delta}$ series ($x = 0$ (LCN); $x = 0.1$ (LCNT-1); $x = 0.2$ (LCNT-2); $x = 0.3$ (LCNT-3); and $x = 0.4$ (LCNT-4)) from impedance measurements in humidified air.

in turn affected by changes in temperature and level of tantalum doping. The results of tantalum doping presented in this work suggest that understanding the impact of structure on the activation energies should rely more on a detailed analysis of distances between proton sites than simply upon the degree of lattice distortion.

The bulk resistance and the corresponding grain boundary resistance obtained from AC impedance spectra below 550 °C are plotted as function of the inverse temperature and shown in Fig. 10a and b, respectively. It should be noted that the bulk and grain boundary resistance data of $La_{0.99}Ca_{0.01}NbO_{4-\delta}$ at 550 °C were not shown in Fig. 10 since this temperature point is above the phase transition temperature (~520 °C). The results show that both the bulk and grain boundary resistance increase with increasing Ta content from 550 °C to 400 °C. In addition, a comparison between Fig. 10a and b reveals that while the bulk dominates the total resistance of $La_{0.99}Ca_{0.01}Nb_{1-x}Ta_xO_{4-\delta}$ above 500 °C, the total conductivity includes contribution from both bulk and grain boundary below 500 °C. These results indicate that grain boundary resistance will not affect the use of $La_{0.99}Ca_{0.01}Nb_{1-x}Ta_xO_{4-\delta}$ electrolyte membranes over a temperature range from 600 °C to 800 °C.

Overall, the phase transition temperature of Ca-doped $LaNbO_{4-\delta}$ was successfully elevated to above 800 °C by partially substituting Nb with Ta, however, the conductivity decreased slightly with increase of Ta content above 750 °C. In addition to performance, the reliability of a device is a critically important consideration for practical applications, and the development of high durability materials or cell components is considered a key technical challenge for SOFCs. While the proton conductivity of Ca-doped $LaNbO_{4-\delta}$ is one order of magnitude lower than the $BaCeO_3$- or $SrCeO_3$-based perovskites, which exhibit a proton conductivity of $\sim 10^{-2}$ S cm^{-1} at operation temperature, the perovskites face a material limitation when operating under CO_2 and H_2O conditions. For Ca-doped $LaNbO_{4-\delta}$, the long-term chemical stability in combination with thin-film growth techniques make it feasible for electrolyte application in high temperature proton conducting fuel cells, in addition to other applications such as hydrogen production and high temperature sensors. Given a power density of 65 mW cm^{-2} was achieved with a 20-μm Ca-doped $LaNbO_{4-\delta}$ electrolyte membrane using traditional SOFC electrode materials in Ref. [10], the performance should be improved by developing a suitable electrode and using 2–5 μm thin film electrolyte membrane. At the same time, the electrolyte cost will be decreased by using a thin-film as compared to thick membranes. However, as we pointed out previously, the use of thin-film devices requires that the CTE of cell components should be highly matched. Partial substitution of Nb with Ta elevates the phase transition temperature from 520 °C for Ca-doped $LaNbO_{4-\delta}$ to above 800 °C for Ca-doped $LaNb_{0.6}Ta_{0.4}O_{4-\delta}$, which means that no huge CTE change will be occurred below 800 °C. Furthermore, the conductivity of Ca-doped $LaNb_{0.6}Ta_{0.4}O_4$ does not differ greatly from Ca-doped $LaNbO_{4-\delta}$ at operation temperature (750–850 °C) according to experimental results. Therefore, based on the high phase transition temperature and the slightly lower conductivity observed in Ca-doped $LaNb_{0.6}Ta_{0.4}O_{4-\delta}$, partial substitution of Nb with Ta improves the viability of this family of materials for use as a thin-film electrolyte in intermediate-temperature SOFCs or in high-temperature electrochemical applications.

4. Conclusion

$La_{0.99}Ca_{0.01}Nb_{1-x}Ta_xO_{4-\delta}$ ($x = 0$–0.5 in steps of 0.1) phases have been structurally characterized both at room temperature and at 800 °C using X-ray powder diffraction. The results showed that with increasing amounts of tantalum substitution up to 0.4 mole formula^{-1} unit a pure monoclinic phase is obtained at room temperature; by $x = 0.5$, the lower solubility of Ta in the monoclinic structure leads to a two-phase mixture of monoclinic and orthorhombic phases. Substituting Nb with Ta increased the monoclinic-to-tetragonal phase transition temperatures of the $La_{0.99}Ca_{0.01}Nb_{1-x}Ta_xO_{4-\delta}$ from ~520 °C for $x = 0$ to near 800 °C for $x = 0.4$. The conductivity decreased slightly from 3.5×10^{-4} S cm^{-1} for $La_{0.99}Ca_{0.01}NbO_{4-\delta}$ to 2.3×10^{-4} S cm^{-1} for $La_{0.99}Ca_{0.01}Nb_{0.6}Ta_{0.4}O_{4-\delta}$ at 850 °C in humidified air; however, at low temperatures, it decreased by nearly one order of magnitude. In addition, while the introduction of Ta onto the Nb site slightly increases the activation energy of the tetragonal phase, it decreases the activation energy for the monoclinic phase.

Acknowledgements

This work was sponsored by the Laboratory Directed Research and Development (LDRD) Program of Oak Ridge National Laboratory, managed by UT-Battelle, LLC, for the U.S. Department of Energy. The XRD work of this research was conducted at CNMS User Facility, which is sponsored by the Division of Scientific User Facilities, Office of Basic Energy Sciences, U.S. Department of Energy. This Research was also supported by Oak Ridge National Laboratory's SHaRE User Facility, which is sponsored by the Office of Basic Energy Sciences, U.S. Department of Energy. Support for Dr. Huq comes from SNS which is managed by UT-Battelle, LLC, under contract DEAC05-00OR22725 for the US Department of

Energy. Dr. Zhonghe Bi and Dr. Jung-Hyun Kim acknowledge the support of the ORISE postdoctoral fellowship.

References

[1] H. Iwahara, Y. Asakura, K. Katahira, M. Tanaka, Solid State Ionics 168 (2004) 299.
[2] S.M. Haile, Acta Materials 51 (2003) 5981.
[3] K.D. Kreuer, Chemistry of Materials 8 (1996) 610.
[4] M.J. Scholten, J. Schoonman, J.C. Miltenburg, H.A.J. Oonk, Solid State Ionics 61 (1993) 83.
[5] K. Katahira, Y. Kohchi, T. Shimura, H. Iwahara, Solid State Ionics 138 (2000) 91.
[6] K.D. Kreuer, Solid State Ionics 97 (1997) 1.
[7] R. Haugsrud, T. Norby, Nature Materials 5 (2006) 193.
[8] R. Haugsrud, T. Norby, Solid State Ionics 177 (2006) 1129.
[9] M.L. Fontaine, Y. Larring, R. Haugsrud, T. Norby, K. Viik, R. Bredesen, Journal of Power Sources 188 (2009) 106.
[10] B. Lin, S. Wang, X. Liu, G. Meng, Journal of Alloys and Compounds 478 (2009) 355.
[11] A. Magrasó, H. Xuriguera, M. Varela, M.F. Sunding, R. Strandbakke, R. Haugsrud, T. Norby, Journal of the American Ceramic Society 93 (2010) 1874.
[12] V.S. Stubican, Journal of the American Ceramic Society 47 (1964) 33.
[13] J.F. Whitney, F.C. Zumsteg, G.A. Jones, Materials Research Bulletin 12 (1977) 17.
[14] L. Jian, C.M. Wayman, Journal of the American Ceramic Society 80 (1997) 803.
[15] F. Vullum, F. Nitsche, S.M. Selbach, T. Grande, Journal of Solid State Chemistry 181 (2008) 2580.
[16] R. Haugsrud, T. Norby, Journal of the American Ceramic Society 90 (2007) 1116.
[17] A.C. Larson, R.B. vonDreele, General Structure Analysis System (GSAS), Los Alamos National Laboratory Report LAUR 86748, 2000.
[18] B.H. Toby, Journal of Applied Crystallography 34 (2001) 210.
[19] H. Fjeld, K. Toyoura, R. Haugsrud, T. Norby, Physical Chemistry Chemical Physics 12 (2010) 10313.
[20] E.V. Arkhipova, M.G. Zuev, L.V. Zolotukhina, Journal of Alloys and Compounds 305 (2000) 297.
[21] L. Jian, C.M. Huang, G.B. Xu, C.M. Wayman, Materials Letters 21 (1994) 105.
[22] Ø. Prytz, J. Taftø, Acta Materials 53 (2004) 297.
[23] R.D. Shannon, Acta Crystallographica A 32 (1976) 751.
[24] M.L. Vrtis, J.D. Jorgensen, D.G. Hinks, Physica B 136 (1986) 489.
[25] T. Mokkelbost, I. Kaus, R. Haugsrud, T. Norby, T. Grande, M. Einarsrud, Journal of the American Ceramic Society 91 (2008) 879.
[26] I. Ahmed, S.G. Eriksson, E. Ahlberg, C.S. Knee, P. Berastegui, L.G. Johansson, H. Rundlöf, M. Karlsson, A. Matic, L. Börjesson, D. Engberg, Solid State Ionics 177 (2006) 1395.
[27] A.R. Potter, R.T. Baker, Solid State Ionics 177 (2006) 1917.
[28] S. Gallini, M. Hänsel, T. Norby, M.T. Colomer, J.R. Jurado, Solid State Ionics 162 (2003) 167.
[29] H. Iwahara, Solid State Ionics 86–88 (1996) 9.
[30] R.J. Phillips, N. Bonanos, F.W. Poulsen, E.Q. Ahlgren, Solid State Ionics 162–163 (1999) 389.